AGU PUBLICATIONS

Geophysical Research Letters

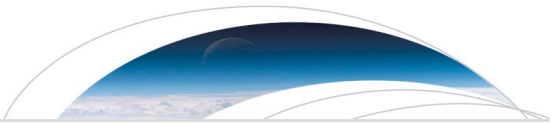

RESEARCH LETTER

10.1002/2014GL062748

Key Points:
- The IMF B_y has an impact on the high-latitude thermospheric density
- Positive/negative B_y effect in NH resembles negative/positive B_y effect in SH
- Thus, the IMF B_y is an important source for the north-south asymmetry

Correspondence to:
Y. Yamazaki,
y.yamazaki@lancaster.ac.uk

Citation:
Yamazaki, Y., M. J. Kosch, and E. K. Sutton (2015), North-south asymmetry of the high-latitude thermospheric density: IMF B_Y effect, *Geophys. Res. Lett.*, *42*, doi:10.1002/2014GL062748.

Received 3 DEC 2014
Accepted 17 DEC 2014
Accepted article online 22 DEC 2014

North-south asymmetry of the high-latitude thermospheric density: IMF B_Y effect

Yosuke Yamazaki[1], Michael J. Kosch[1,2], and Eric K. Sutton[3]

[1]Department of Physics, Lancaster University, Lancaster, UK, [2]South African National Space Agency, Hermanus, South Africa, [3]AFRL, Kirtland Air Force Base, New Mexico, USA

Abstract Previous studies have established that the *y* component of the interplanetary magnetic field (IMF B_y) plays a role in the north-south asymmetry of the high-latitude plasma convection and wind. The effect of the positive/negative IMF B_y in the Northern Hemisphere resembles the effect that the negative/positive IMF B_y would have in the Southern Hemisphere. In this study, we demonstrate that the IMF B_y effect can also contribute to the hemispheric asymmetry of the thermospheric density. We use high-accuracy air drag measurements from the CHAllenging Minisatellite Payload (CHAMP) satellite and SuperMAG *AE* index during the period 2001–2006 to examine the response of the high-latitude thermospheric density to geomagnetic activity. Our statistical analysis reveals that the density response at 400 km is greater in the Southern Hemisphere under positive IMF B_y conditions, and greater in the Northern Hemisphere under negative IMF B_y conditions. The results suggest that the IMF B_y effect needs to be taken into account in upper atmospheric modeling for an accurate description of high-latitude densities during periods of enhanced geomagnetic activity.

1. Introduction

The interaction between the solar wind and magnetosphere generates electric fields in the high-latitude ionosphere. These electric fields cause the ionospheric plasma to convect around the regions of positive and negative electric potentials. It is well known that the patterns of these convection "cells" are dependent on the strength and orientation of the IMF [e.g., *Cousins and Shepherd*, 2010]. Particularly, the role of the IMF B_y has been found to produce an asymmetry between the Northern Hemisphere and Southern Hemisphere convection patterns. For a nonzero IMF B_y condition, the cell patterns in the Northern Hemisphere resemble those in the Southern Hemisphere for the opposite sense of the IMF B_y.

The neutral gas in the high-latitude regions tends to be accelerated, or "dragged", in the direction of the rapid motion of the ions due to collisional interactions between plasmas and neutrals. This ion drag effect brings about similarities in the patterns of high-latitude thermospheric wind and ion convection [e.g., *Richmond and Lu*, 2000]. *Förster et al.* [2008] showed that the IMF B_y effect can cause a north-south asymmetry in the high-latitude thermospheric wind in a similar manner as in the ion convection.

The IMF B_y effect on the wind may have a broad impact on the neutral atmosphere. For example, changes in the horizontal wind system can cause the vertical motion of the air, which leads to adiabatic heating or cooling of the gas. Therefore, it is possible that the temperature, composition, and mass of the upper atmosphere are altered as a result of the IMF B_y effect on the wind, although it is difficult to predict what and how much the actual variations might be.

Crowley et al. [2006] used a coupled thermosphere-ionosphere general circulation model to study the IMF B_y effect on the thermosphere. They ran simulations with different ion convection patterns representative of different IMF B_y conditions. Their results suggested that the density distribution in the high-latitude thermosphere systematically changes when the ion convection pattern is changed. Although efforts have also been made to provide observational evidence for the IMF B_y effect on the thermospheric density [e.g., *Immel et al.*, 1997, 2006; *Kwak et al.*, 2009], an important piece of evidence has been missing, i.e., the hemispheric asymmetry associated with the IMF B_y effect. In this paper, we will provide evidence that the north-south asymmetry of the high-latitude thermospheric density can arise from the IMF B_y effect.

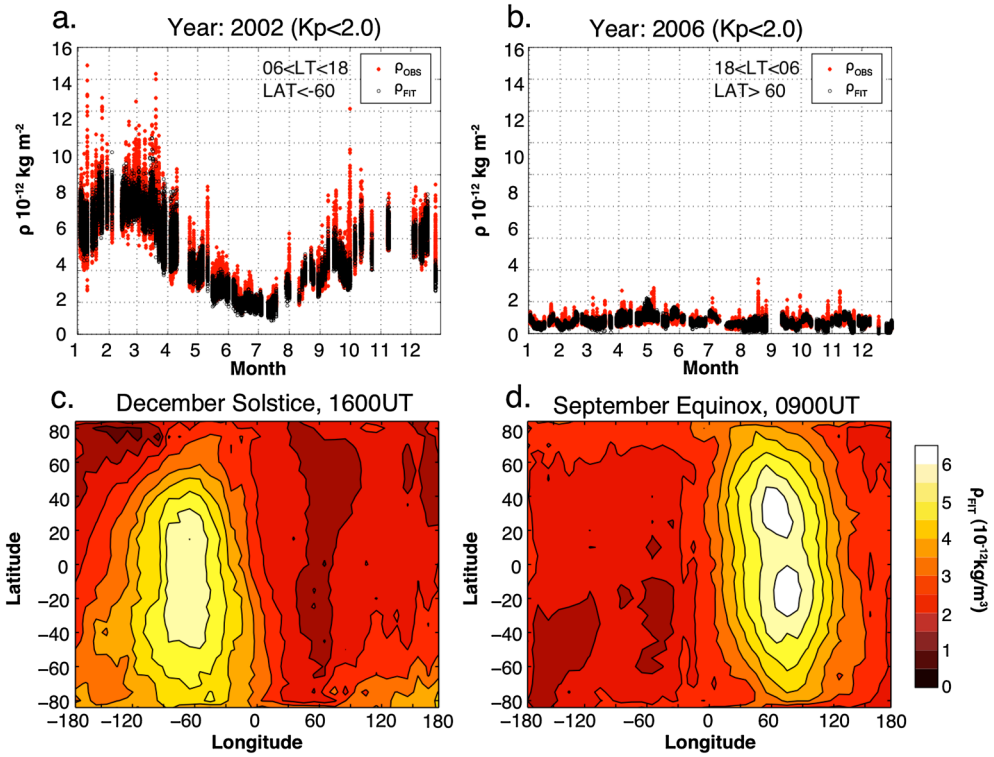

Figure 1. (a) Quiet time thermospheric densities at 400 km in the Southern Hemisphere (poleward of −60°) for local times between 0600 and 1800 h for the year 2002. The red dots represent observations, while the black circles represent the fit to the data as expressed by equation (1). (b) The same as Figure 1a but in the Northern Hemisphere (poleward of 60°) for local times between 1800 and 0600 h for the year 2006. (c) Latitude versus longitude distribution of ρ_{FIT} at 1600 UT for the December solstice and for the average solar activity condition corresponding to P ~110 sfu. (d) The same as Figure 1c but at 0900 UT for the September equinox.

2. Data Analysis

We use air drag measurements by the CHAMP satellite [*Reigber et al.*, 2002] to derive the air density at 400 km for the period from July 2000 to December 2006. The density retrieval procedures and error evaluations were detailed in *Sutton* [2008]. We first determine quiet time densities, which will be used later as a baseline of density perturbations. For this purpose, the analysis is restricted to quiet geomagnetic conditions defined as $Kp < 2$. The quiet time data are divided into 1260 bins according to the geographical location of measurements in a latitude-longitude grid of 5° × 10°. The data in each bin are expressed as a product of functions of solar activity, season, and local time (LT). The empirical formula is given by

$$\rho_{FIT} = Re\left\{\sum_{l}\sum_{m}\sum_{n} C_{lmn}(MgII)^{l} e^{i\left(m\frac{2\pi DoY}{365.24}\right)} e^{i\left(n\frac{2\pi LT}{24}\right)}\right\}, \quad (1)$$

where $l = 0, 1$; $m = -3, -2, \ldots, 3$; and $n = -4, -3, \ldots, 4$. The *MgII* index [*Viereck et al.*, 2001] is used as a proxy for solar EUV activity. Studies have shown that the *MgII* index is a good proxy for the solar activity influence on the thermospheric density [e.g., *Solomon et al.*, 2011]. The dependence on day of year (*DoY*) represents seasonal variations, including annual, semiannual, and terannual components. The local time variation includes 24, 12, 8, and 6 h components. The 126 coefficients C_{lmn} are determined on the basis of least squares fitting in the same way as *Yamazaki et al.* [2012]. The goodness of fit R^2, which is defined as the square of the correlation coefficient between the original data and fit, is found to be reasonably high at any geographical location. The average R^2 is 0.96 at high latitudes (poleward of ±60° latitude).

Figure 1 demonstrates spatial and temporal variabilities of ρ_{FIT}. Figures 1a and 1b compare ρ_{FIT} against the original data. Figure 1a shows quiet time densities at high latitudes in the Southern Hemisphere for the year 2002 (near-solar maximum) for local times between 0600 and 1800 h, while Figure 1b shows Northern Hemisphere densities for the year 2006 (near-solar minimum) for different local times. Density distributions are

presented in Figures 1c and 1d for different seasons and universal times, for an average solar activity condition corresponding to $P \sim 110$ sfu. Here P represents the solar activity index by *Richards et al.* [1994], and sfu stands for solar flux unit. Examples presented in Figure 1 illustrate basic features of quiet time thermospheric density known from previous studies [see, e.g., *Qian and Solomon*, 2012, for a review].

We define density perturbations $\Delta\rho$ as the difference between the measurements and quiet time values as expressed by (1). The density perturbations are analyzed in the Magnetic Apex coordinate system [*Richmond*, 1995] as a function of magnetic latitude (MLAT) and magnetic local time (MLT) with a grid size of $5^\circ \times 1$ h.

We use hourly values of the SuperMAG *AE* index [*Newell and Gjerloev*, 2011] to characterize high-latitude geomagnetic activity. Studies have shown that the typical response time of thermospheric densities to geomagnetic activity is less than 2 h at high latitudes and about 4 h at low latitudes [*Sutton et al.*, 2009; *Ritter et al.*, 2010]. Since our study focuses on the high-latitude densities, we use *AE* values averaged for the present hour and 1 h prior. Our average quiet time densities correspond to an *AE* index of approximately 150 nT, and thus, the density perturbations are examined as a function of $AE_d = AE - 150$ for positive values of this parameter. The density perturbations are binned in 50 nT window of AE_d up to 400 nT, and into one bin for larger values. A linear regression analysis is then performed using the median value of $\Delta\rho$ and AE_d in each bin. This median filter effectively eliminates outliers.

3. Results and Discussion

Figure 2a shows an example of results obtained from the linear regression analysis described above. The results are for a high-latitude dayside region in the Southern Hemisphere ($12 \leq$ MLT < 13 and $-75 \leq$ MLAT < -70) for relatively high solar activity conditions ($P \geq 110$ sfu). The error bars have a length of twice the standard deviation of $\Delta\rho$ in each bin. Despite the large scatter, the median density perturbations tend to linearly increase with an increase of AE_d, indicating that the day-to-day variability, unrelated to geomagnetic activity, is effectively averaged out. Figure 1b shows another example of results obtained for a high-latitude nightside region in the Northern Hemisphere ($22 \leq$ MLT < 23 and $70 \leq$ MLAT < 75) for $P < 110$ sfu.

Figures 2c and 2f show the density perturbations normalized to $AE = 400$ nT under $P \geq 110$ sfu conditions in the Northern Hemisphere and Southern Hemisphere, respectively. The results are displayed in the MLAT and MLT coordinates. Figures 2d and 2g show the corresponding standard deviations, derived from our linear regression analysis. The standard deviations are typically about 1×10^{-13} kg m^{-2} but occasionally large, indicating an inaccurate linear regression fit. In the rest of the paper, we do not show the standard deviations for each plot, but the density results are rejected if the standard deviation exceeds an arbitrary threshold of 3×10^{-13} kg m^{-2}.

Figures 2c and 2f reveal a strong density response in the dayside region. The dayside high-latitude thermosphere is where the cusp region density enhancement is often observed [e.g., *Lühr et al.*, 2004]. It should be noted, however, that the cusp region density enhancement generally occurs in a much narrower region with a half width of a few hundred kilometers. Thus, the enhanced dayside response shown in Figures 2c and 2f could be due to other processes. The density response is also relatively large in the premidnight sector (20–24 MLT), where the substorm onset often occurs. The density response is least significant around the dawn sector (4–7 MLT) in both hemispheres.

Crowley et al. [1996], using a thermosphere-ionosphere general circulation model, predicted the existence of organized density structures, or "density cells", in the high-latitude thermosphere. Those cells are the regions where the density is locally increased or decreased from the background level. Their model showed two to four high- and low-density cells with a size of 1000–2000 km in diameter at 140 and 200 km altitudes. Our results in Figures 2c and 2f seem to indicate such organized structures mainly with a high-density cell in the noon sector and a low-density cell in the dawn sector. It should be pointed out, however, that in the simulations by *Crowley et al.* [1996], the density cells decayed with height and no structure was evident above 350 km.

Figures 2e and 2h are the same as Figures 2c and 2f except for $P < 110$. A comparison between the results for $P \geq 110$ and $P < 110$ indicate that high-latitude density perturbations are larger during higher solar flux periods, for the same level of geomagnetic activity. This is owing to the fact that the magnitude

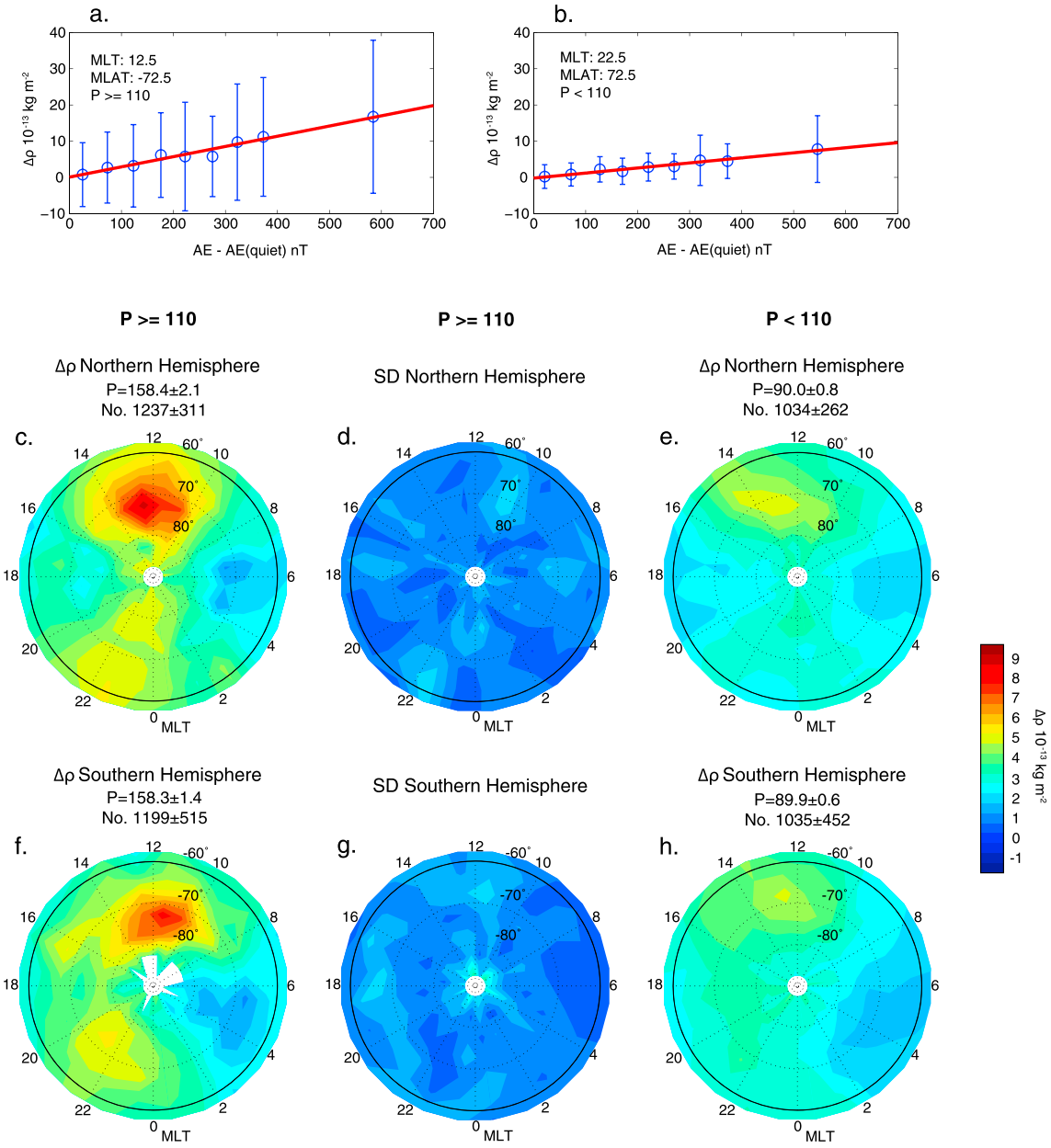

Figure 2. (a, b) Examples of the relationship between AE_d and density perturbations $\Delta\rho$ at 400 km. (c, f) Distributions of the high-latitude density perturbations $\Delta\rho$ at 400 km for $AE = 400$ nT and $P \geq 110$ sfu. The average value of P and its standard deviation (in sfu) are also indicated, along with the average number of the data points and its standard deviation. (d, g) Distributions of the standard deviation (SD) for the high-latitude density perturbations $\Delta\rho$ at 400 km for $AE = 400$ nT and $P \geq 110$ sfu. (e, h) The same as Figures 2c and 2f but for $P < 110$ sfu.

of density perturbations tends to increase with the background density. It is interesting to note that the density response in the dawn sector shows the opposite solar activity dependence. That is, the normalized density perturbation is slightly lower for the higher solar activity condition.

Figure 3 illustrates the dependence of the high-latitude thermospheric density perturbations on the IMF clock angle for $AE = 400$ nT. The IMF clock angle was derived from hourly values of OMNI solar wind data at the Earth's bow shock nose. We define θ as the IMF clock angle averaged for the present hour and 1 h prior. (As mentioned, the AE index is also averaged for the same interval.) Binning ranges for θ are as follows: (a, d) $-70° \leqq \theta < 70°$, (b, e) $250° \leqq \theta < 290°$, (c, f) $205° \leqq \theta < 250°$, (g, j) $155° \leqq \theta < 205°$, (h, k) $110° \leqq \theta < 155°$, (i, l) $70° \leqq \theta < 110°$. We initially attempted to separate the $B_z > 0$ data into smaller bins, but it proved difficult to obtain the normalized densities because $B_z > 0$ leads AE_d to be negative, and thus, our linear regression analysis tends to be unsuccessful.

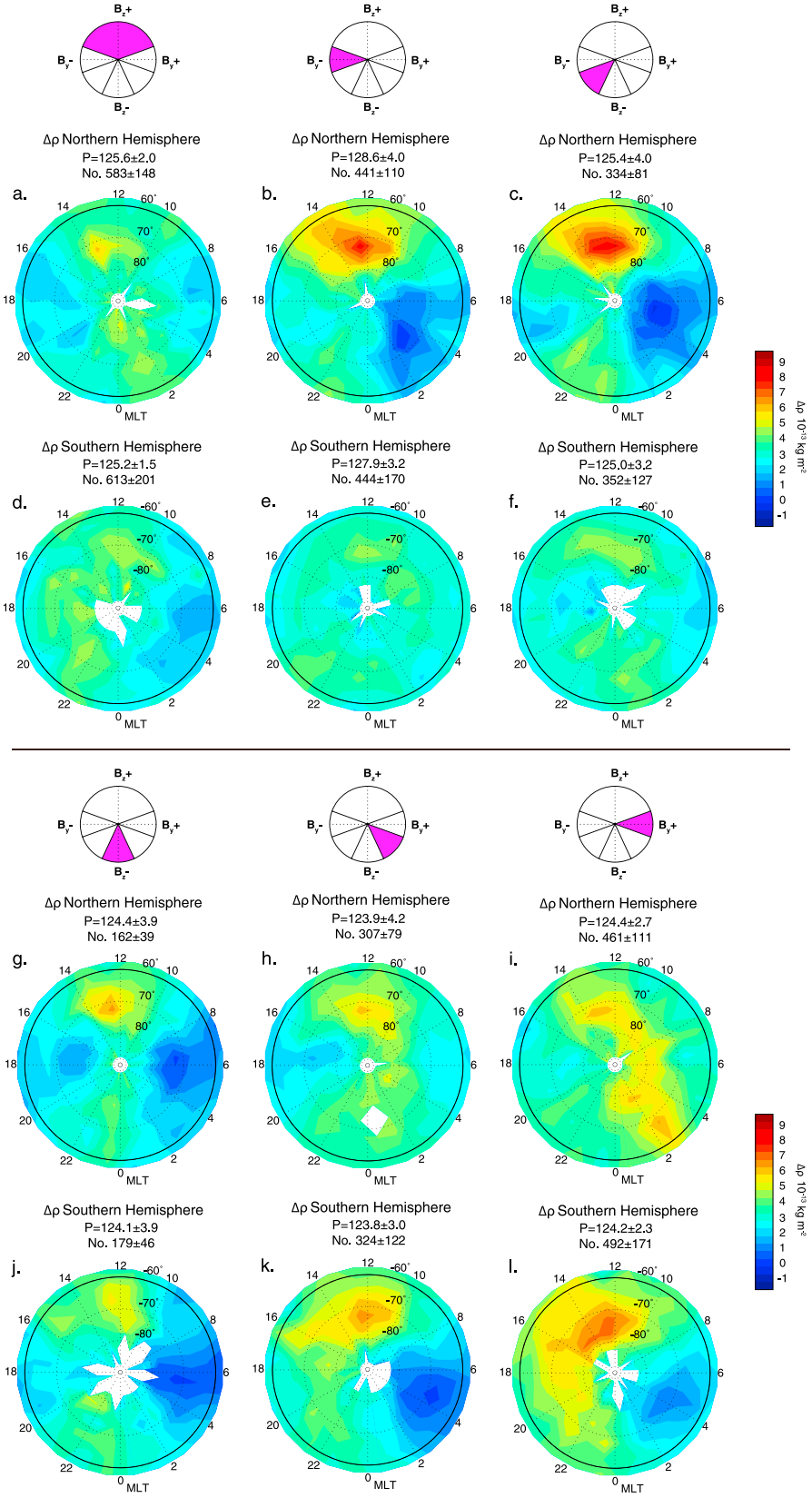

Figure 3. The high-latitude density perturbations $\Delta\rho$ at 400 km for AE = 400 nT for (a, d) $-70° \leqq \theta < 70°$, (b, e) $250° \leqq \theta < 290°$, (c, f) $205° \leqq \theta < 250°$, (g, j) $155° \leqq \theta < 205°$, (h, k) $110° \leqq \theta < 155°$, and (i, l) $70° \leqq \theta < 110°$. Binning ranges for θ are indicated in the B_y-B_z plane on the top of Northern Hemisphere results.

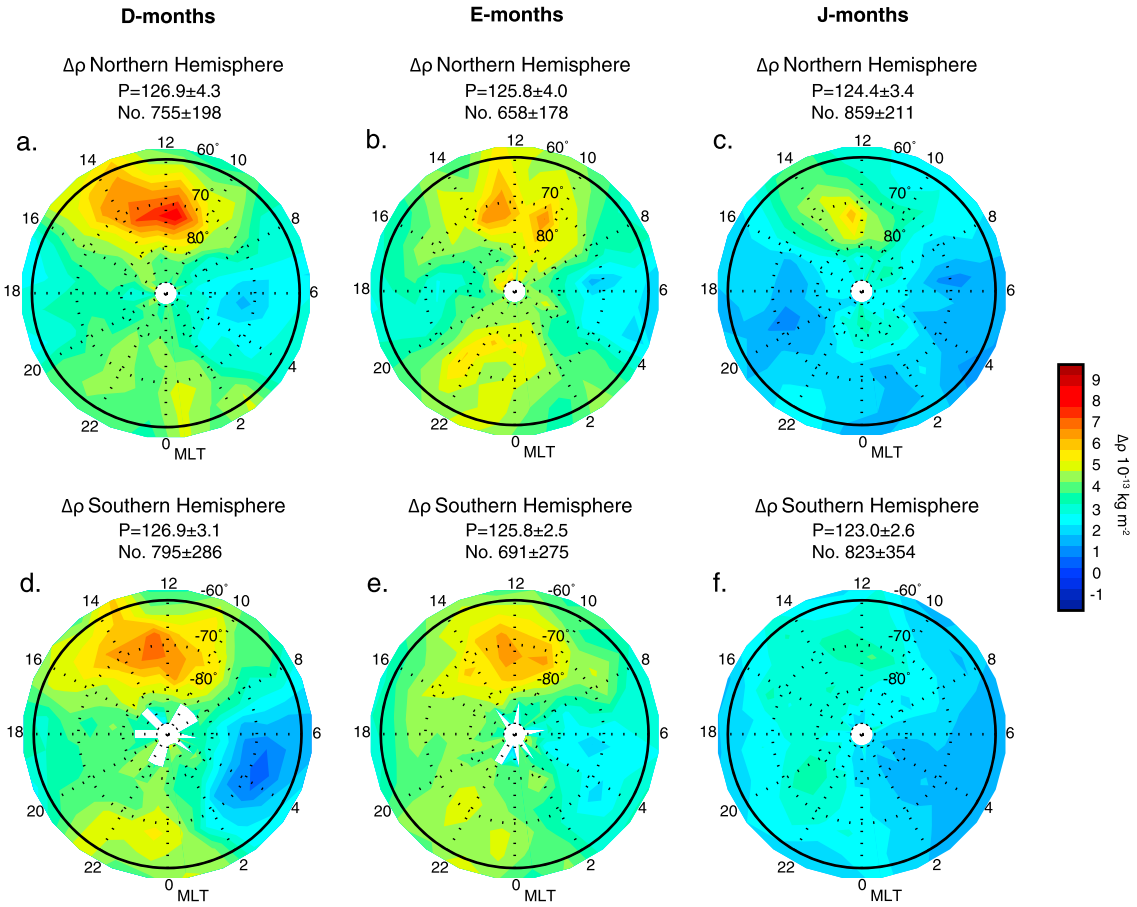

Figure 4. The dependence of the high-latitude density perturbations $\Delta\rho$ at 400 km on the season for AE = 400 nT.

The results in Figure 3 indicate that the IMF B_y direction is an important factor for the north-south asymmetry of the high-latitude density response to geomagnetic activity. It can be seen that negative and positive B_y conditions are preferred for the Northern Hemisphere and Southern Hemisphere density cells to develop. Previously, *Crowley et al.* [2006] numerically predicted that a polarity change of the IMF from $B_y < 0$ to $B_y > 0$ causes a reduction in the magnitude of the density cells in the Northern Hemisphere. The sense of the effect is consistent with our results. However, their study was limited only up to 200 km, and thus, the direct comparison with our results is not possible.

In Figure 3, the dayside density response to the IMF B_y is greater than the response to the negative IMF B_z. The interpretation for this needs to be made carefully, as the IMF B_z correlates with the AE index. For example, when the IMF clock angle is 180°, the AE index is likely to be higher than when the IMF clock angle is 90°. Thus, the actual dayside density perturbations for $\theta = 180°$ are, on average, greater than those for $\theta = 90°$.

It is noted that the density perturbation in the dawn sector is sometimes negative. This means that the densities in those regions tend to decrease with increasing geomagnetic activity and therefore indicates a strong cooling effect against heating due to auroral processes. The effect may be explained by enhanced production of nitric oxide during periods of increased geomagnetic activity. Nitric oxide acts to increase the radiative cooling of the thermosphere and thus causes a reduction of local densities [e.g., *Lei et al.*, 2012; *Knipp et al.*, 2013]. The dawn sector is where pulsating auroras often appear [*Omholt*, 1971]. The pulsating aurora is caused by precipitation of hard electrons, which penetrate into the upper mesosphere and thus add to production of nitric oxide.

Figure 4 shows the seasonal dependence of the high-latitude density perturbations. The data were grouped into three seasonal bins: D months (November–February), J months (May–August), and E months (March,

April, September, and October). The results do not show a strong north-south asymmetry unlike the case for nonzero IMF B_y conditions.

There is an apparent annual modulation in the density response to geomagnetic activity. That is, the overall density perturbations are smaller during the J months than D months for the same level of geomagnetic activity. The background thermospheric density tends to be globally low during the J months [e.g., *Qian et al.*, 2009], which may be a reason for the weak response during the J months. Also, the *AE* index, which is based on the Northern Hemisphere magnetometer data, undergoes an annual variation [e.g., *Singh et al.*, 2013], and it may affect our results.

4. Summary and Conclusions

Earlier studies have established the role of the IMF B_y in producing a hemispheric asymmetry of the high-latitude ion convection and wind. The effect of positive/negative B_y in the Northern Hemisphere has been found to be similar to the effect of negative/positive B_y in the Southern Hemisphere. We have investigated the possible contribution of the IMF B_y to the north-south asymmetry of the high-latitude thermospheric density response to geomagnetic activity by using air drag measurements from the CHAMP satellite. The results of our statistical analysis revealed that such an effect does exist.

We have shown that the high-latitude disturbance density structure is often characterized by a high-density region around the noon sector and a low-density region in the dawn sector. They have the features of the density cells, which has been theoretically predicted but only below 350 km [*Crowley et al.*, 1996, 2006]. It was found that the cell structures in the Northern Hemisphere and Southern Hemisphere become more evident under negative and positive B_y conditions, respectively. This is qualitatively consistent with simulation results by *Crowley et al.* [2006], although their simulations were limited up to 200 km. Their model used different patterns of the high-latitude ion convection according to the B_y input, and thus, changes in the density were mainly due to the ion drag effect on the neutral wind. The model used by *Crowley et al.* [2006] was, however, unable to examine the possibility that the IMF B_y might cause a hemispheric asymmetry in the energy input from the magnetosphere. For example, magnetohydrodynamic simulations of the coupled solar wind-magnetosphere-ionosphere system by *Tanaka* [2001] predicted a hemispheric asymmetry in the distribution of high-latitude field-aligned currents under nonzero IMF B_y conditions. Further numerical investigations will be necessary to clarify the mechanism for the IMF B_y effect on the thermospheric density.

The IMF B_y effect is not considered in most empirical models of the thermosphere. Our results suggest that the IMF B_y effect needs to be taken into account for an accurate description of the density response to geomagnetic activity, especially at high latitudes.

The seasonal effect was another possible source for the hemispheric asymmetry. However, we did not find evidence of the seasonal effect on the north-south asymmetry of the high-latitude density perturbations. A more comprehensive study is planned to examine the combined effect of the seasons and IMF B_y, e.g., the seasonal effect on the north-south asymmetry due to the IMF B_y effect.

Finally, the results in this paper represent only the average state and do not necessarily agree with individual cases. The large scatter of the data, which was found in the binning process (see Figures 2a and 2b), indicates that there are many data points that deviate from the average results. Therefore, it is important to be aware of other sources of variability as well, when interpreting case study results.

Acknowledgments
The *Kp* index was provided by the German Research Center for Geosciences, GFZ (http://www.gfz-potsdam.de/en/home). The *MgII* index was provided by the Institute of Environmental Physics, University of Bremen (http://www.iup.uni-bremen.de/gome/gomemgii.html). The $F_{10.7}$ index was provided by the Herzberg Institute of Astrophysics. The hourly solar wind data were obtained from the NASA OMNIweb database (http://omniweb.gsfc.nasa.gov/). The SuperMAG *AE* index was downloaded from the SuperMAG website (http://supermag.jhuapl.edu/). For the ground magnetometer data we gratefully acknowledge: Intermagnet; USGS, Jeffrey J. Love; CARISMA, Ian Mann; CANMOS; The S-RAMP Database, K. Yumoto and K. Shiokawa; The SPIDR database; AARI, Oleg Troshichev; The MACCS program, M. Engebretson, Geomagnetism Unit of the Geological Survey of Canada; GIMA; MEASURE, UCLA IGPP, and Florida Institute of Technology; SAMBA, Eftyhia Zesta; 210 Chain, K. Yumoto; SAMNET, Farideh Honary; The institutes who maintain the IMAGE magnetometer array, Eija Tanskanen; PENGUIN; AUTUMN, Martin Conners; DTU Space, Jürgen Matzka; South Pole and McMurdo Magnetometer, Louis J. Lanzarotti and Alan T. Weatherwax; ICESTAR; RAPIDMAG; PENGUIn; British Artarctic Survey; McMac, Peter Chi; BGS, Susan Macmillan; Pushkov Institute of Terrestrial Magnetism, Ionosphere and Radio Wave Propagation (IZMIRAN); GFZ, Monika Korte; SuperMAG, Jesper W. Gjerloev. Y.Y. and M.J.K. were supported by NERC grant NE/K01207X/1.

The Editor thanks Stanley Solomon and an anonymous reviewer for their assistance in evaluating this paper.

References

Cousins, E. D. P., and S. G. Shepherd (2010), A dynamical model of high-latitude convection derived from SuperDARN plasma drift measurements, *J. Geophys. Res.*, *115*, A12329, doi:10.1029/2010JA016017.

Crowley, G., J. Schoendorf, R. G. Roble, and F. Marcos (1996), Cellular structures in the high-latitude thermosphere, *J. Geophys. Res.*, *101*, 211–223.

Crowley, G., T. J. Immel, C. L. Hackert, J. Craven, and R. G. Roble (2006), Effect of IMF BY on thermospheric composition at high and middle latitudes: 1. Numerical experiments, *J. Geophys. Res.*, *111*, A10311, doi:10.1029/2005JA011371.

Förster, M., S. Rentz, W. Köhler, H. Liu, and S. E. Haaland (2008), IMF dependence of high-latitude thermospheric wind pattern derived from CHAMP cross-track measurements, *Ann. Geophys.*, *26*, 1581–1595, doi:10.5194/angeo-26-1581-2008.

Immel, T. J., J. D. Craven, and L. A. Frank (1997), Influence of IMF By on large-scale decreases of O column density at middle latitudes, *J. Atmos. Terr. Phys.*, *59*, 725–736.

Immel, T. J., G. Crowley, C. L. Hackert, J. D. Craven, and R. G. Roble (2006), Effect of IMF By on thermospheric composition at high and middle latitudes: 2. Data comparisons, *J. Geophys. Res.*, *111*, A10312, doi:10.1029/2005JA011372.

Knipp, D., L. Kilcommons, L. Hunt, M. Mlynczak, V. Pilipenko, B. Bowman, Y. Deng, and K. Drake (2013), Thermospheric damping response to sheath-enhanced geospace storms, *Geophys. Res. Lett.*, *40*, 1263–1267, doi:10.1002/grl.50197.

Kwak, Y.-S., A. D. Richmond, Y. Deng, J. M. Forbes, and K.-H. Kim (2009), Dependence of the high-latitude thermospheric densities on the interplanetary magnetic field, *J. Geophys. Res.*, *114*, A05304, doi:10.1029/2008JA013882.

Lei, J., A. G. Burns, J. P. Thayer, W. Wang, M. G. Mlynczak, L. A. Hunt, X. Dou, and E. Sutton (2012), Overcooling in the upper thermosphere during the recovery phase of the 2003 October storms, *J. Geophys. Res.*, *117*, A03314, doi:10.1029/2011JA016994.

Lühr, H., M. Rother, W. Köhler, P. Ritter, and L. Grunwaldt (2004), Thermospheric up-welling in the cusp region: Evidence from CHAMP observations, *Geophys. Res. Lett.*, *31*, L06805, doi:10.1029/2003GL019314.

Newell, P. T., and J. W. Gjerloev (2011), Evaluation of SuperMAG auroral electrojet indices as indicators of substorms and auroral power, *J. Geophys. Res.*, *116*, A12211, doi:10.1029/2011JA016779.

Omholt, A. (1971), *The Optical Aurora*, Springer, New York.

Qian, L., and S. C. Solomon (2012), Thermospheric density: An overview of temporal and spatial variations, *Space Sci. Rev.*, *168*, 147–173, doi:10.1007/s11214-011-9810-z.

Qian, L., S. C. Solomon, and T. J. Kane (2009), Seasonal variation of thermospheric density and composition, *J. Geophys. Res.*, *114*, A01312, doi:10.1029/2008JA013643.

Reigber, C., H. Lühr, and P. Schwintzer (2002), CHAMP mission status, *Adv. Space Res.*, *30*, 129–134.

Richards, P. G., J. A. Fennelly, and D. G. Torr (1994), EUVAC: A solar EUV Flux Model for aeronomic calculations, *J. Geophys. Res.*, *99*(A5), 8981–8992, doi:10.1029/94JA00518.

Richmond, A. D. (1995), Ionospheric electrodynamics using magnetic apex coordinates, *J. Geomagn. Geoelectr.*, *47*, 191–212.

Richmond, A. D., and G. Lu (2000), Upper-atmospheric effects of magnetic storms: A brief tutorial, *J. Atmos. Sol. Terr. Phys.*, *62*, 1115–1127.

Ritter, P., H. Lühr, and E. Doornbos (2010), Substorm-related thermospheric density and wind disturbances derived from CHAMP observations, *Ann. Geophys.*, *28*, 1207–1220, doi:10.5194/angeo-28-1207-2010.

Singh, A. K., R. Rawat, and B. M. Pathan (2013), On the UT and seasonal variations of the standard and SuperMAG auroral electrojet indices, *J. Geophys. Res. Space Physics*, *118*, 5059–5067, doi:10.1002/jgra.50488.

Solomon, S. C., L. Qian, L. V. Didkovsky, R. A. Viereck, and T. N. Woods (2011), Causes of low thermospheric density during the 2007–2009 solar minimum, *J. Geophys. Res.*, *116*, A00H07, doi:10.1029/2011JA016508.

Sutton, E. K. (2008), Effects of solar disturbances on the thermosphere densities and winds from CHAMP and GRACE satellite accelerometer data, PhD dissertation, Univ. of Colo., Boulder, Colo.

Sutton, E. K., J. M. Forbes, and D. J. Knipp (2009), Rapid response of the thermosphere to variations in Joule heating, *J. Geophys. Res.*, *114*, A04319, doi:10.1029/2008JA013667.

Tanaka, T. (2001), Interplanetary magnetic field B_y and auroral conductance effects on high-latitude ionospheric convection patterns, *J. Geophys. Res.*, *106*(A11), 24,505–24,516, doi:10.1029/2001JA900061.

Viereck, R., L. Puga, D. McMullin, D. Judge, M. Weber, and W. K. Tobiska (2001), The Mg II index: A proxy for solar EUV, *Geophys. Res. Lett.*, *28*, 1343–1346, doi:10.1029/2000GL012551.

Yamazaki, Y., A. D. Richmond, and K. Yumoto (2012), Stratospheric warmings and the geomagnetic lunar tide: 1958–2007, *J. Geophys. Res.*, *117*, A04301, doi:10.1029/2012JA017514.